(Received 18 November 2025, Accepted 10 December 2025, Scheduled 27 December 2025)

Compact Dual-Band SIW Bandpass Filter Featuring Reconfigurability for Multi-Application Scenarios

Amjad A. Al-Rahmah* and Bashar J. Hamza

Department of Communications Technical Engineering, Al-Najaf Technical Engineering College/Najaf Al-Furat Al-Awsat Technical University ATU, Najaf 54001, Republic of Iraq

ABSTRACT: The proposed compact dual-band SIW BPF features reconfigurable center frequency and bandwidth, providing two passbands around 2.7 GHz and 4.7 GHz. The lower band targets S-band weather and air-traffic-control radar systems, whereas the upper band covers the 5G NR n79 band, enabling multi-application use in radar and sub-6 GHz 5G wireless communication, utilizing independent reconfigurable methods facilitated by PIN diodes. The suggested design exhibits compact dimensions of $0.21\lambda_g \times 0.48\lambda_g$, a minimal insertion loss of 1.5 dB, and a substantial return loss of 14 dB. Advanced design methodologies, including eigenmode analysis, were utilized to attain precise selectivity and computing of coupling matrix. The engineered filter demonstrates superior performance, with outcomes closely aligning with models, and guarantees little interference with suppression up to 8 GHz. The tuning mechanism provides versatility by independently modifying the operating frequencies of the first and second band, rendering the design very flexible for dynamic wireless communication settings. This study emphasizes a robust and effective answer for contemporary mobile communication systems.

1. INTRODUCTION

To meet the demands of advanced wireless communication systems, low-loss, high-selectivity filters (with high Q-factor resonators) have become essential components. Integrated Substrate Waveguide (SIW) filter offers features such as ease of manufacturing, high endurance, integration, and high linearity, making it an excellent choice for high-performance microfiltration [1]. Initially, traditional filters operated within fixed bands, whether they were single-band [2], dual-band [3], or tri-band [4]. However, the increasing demand for diverse devices in various fields and at relatively small sizes led to the introduction of the concept of reconfiguration filters. Reconfigurable filters are implemented in several ways. In [5], a reconfigurable Band Pass Filter (BPF) used metallic liquid. Ref. [6] utilized the mechanical method by inserting screws inside cavity Substrate Integrated Waveguide (SIW) BPF. In [7], independent of the the mechanical method, the electronic approach, being the most common, relies on varactors and PIN diodes. However, fixed band filters no longer have the flexibility to meet the demands of modern technologies, and it has become necessary to adopt multi-functional filters within a single element.

In [8], a SIW filter is proposed, which is a tunable, multi-mode BPF based on a series of in-line coaxial resonators with a special section for generating zero-transmission (TZ) points, also based on a coaxial resonator. The paper presented two topologies for achieving the Coupling Routing Diagram (CRD): Topology A, which uses parallel LC resonators, and Topology B, which combines parallel and series resonators. Topology B was then applied using a SIW structure with a new component to generate zero-transition points. The prototype demonstrated outstanding performance, including central frequency tuning between 1.24 and 1.8 GHz (1.5 : 1 tuning ratio), bandwidth tuning between 190 and 78 MHz (2.44 : 1 tuning ratio), as well as self-extinguishing with more than 30 dB of isolation within the range of 0.75 to 2.25 GHz. Moreover, in [9], a balanced dual-band, dual-mode, compact, dual-substrate SIW balanced BPF with intrinsic Common Mode (CM) suppression was designed based on a single SIW circular cavity equipped with vias and slots. These disturbances are used to tune TE_{010} and TE_{110} resonant modes (a pair of degenerate modes) and TE_{210} circular cavity and thus can be employed to create two Differential-Mode (DM) passbands with the independent tuning of center frequencies and bandwidths of each. The SIW can be viewed as a natural balun possessing self-suppression of the common signal. Furthermore, a planar differential excitation structure is designed to excite the tunable SIW cavity, such that Common-Mode noise cannot excite the cavity due to its hybrid electromagnetic boundary properties.

Ref. [10] presents a method for designing SIW-based dual-band BPFs and diplexers, with improved wide stopband performance, by leveraging intrinsic mode suppression, and the design allows for the suppression of unwanted anomalous modes by optimally positioning internal coupling windows and external ports. This approach optimizes blocked bandwidth and rejection levels while maintaining a compact circular size without increasing input loss. The study involved the synthesis of two SIW-type duplexing at frequencies of 1.225 GHz and 1.5 GHz, along with a dual-band pass-through reconfigurable filter at a frequency of 1.425 GHz. This resulted in a blocked band extension of up to $1.79\,f_0$ with a rejection level of 24 dB, $2.05\,f_0$

* Corresponding author: Amjad A. Al-Rahmah (amjadabdulsatar@atu.edu.iq).

with a rejection level of 20 dB for the duplexing, and $2.34f_0$ for the dual-band BPF filter.

Ref. [11] introduces a dual-band quasi-elliptic filter design that leverages a hybrid combination of SIW and microstrip technologies. The filter operates at central frequencies of 8 GHz and 10 GHz, using TE_{101} and TE_{201} resonant modes to achieve a compact size, independent coupling paths, and high selectivity. Two pairs of Uniform Impedance Resonators (UIRs) are used to couple the modes, simplifying the design process and optimizing performance. Measured results confirm low insertion loss, high return loss, and precise control of TZs, which enhance out-of-band rejection. The hybrid filter design presents an advanced solution for achieving high selectivity and miniaturization in dual-band filters, though minor deviations in frequency response and optimization complexity pose some challenges. This research provides valuable insights into next-generation filter designs suitable for multi-band communication systems.

In accordance to these necessities, this paper presents a compact and highly Reconfigurable Dual-Band Bandpass Filter (DB-BPF) designed to meet the requirements of modern wireless communication systems. The proposed structure employs a SIW cavity to achieve high performance. The filter utilizes a modified Complementary Split-Ring Resonator (CSRR) slot as the main resonating element, optimized to enhance coupling and operation frequency control. To realize an independent reconfigurable SIW filter across both passbands, multiple PIN diodes are integrated into the resonator and coupling paths, enabling wide and independent reconfiguration over each operating band.

A rigorous design methodology based on the insertion loss technique, coupling matrix, and eigenmode analysis was applied to accurately model and optimize the filter behavior. Theoretical predictions were verified through full-wave simulations and experimental measurements. The fabricated prototype demonstrates wide reconfigurability, low insertion loss, compact size, and high isolation between the two independently reconfigurable bands. The proposed design outperforms previously reported dual-band BPFs in terms of compactness, flexibility, and independent dual-band control.

2. DUAL BAND BANDPASS FILTER CONSTRUCTED ON LOADED SUBSTRATE INTEGRATED WAVEGUIDE WITH COMPLEMENTARY SPLIT RING RESONATORS (CSRR)

This section delineates the stages of the creation of a first-order digital bandpass filter. The proposed filter employs an insertion loss design methodology to determine the theoretical response and fundamental low-pass parameters of the filter [12]. This paper employs a design method commonly used for creating a single-band Chebyshev bandpass filter of any order, Return Loss (RL) level, Fractional Bandwidth (FBW), and Center Frequency (CF). However, to adapt this method for designing a dual-band BPF, a multi-mode resonator with independent mode control is required, enabling the application of the superposition theorem for the independent design of a compact dual-band BPF. Consequently, the suggested design methodology can be employed to create a multi-band bandpass filter with any filter order, fractional bandwidth, and return loss level.

The specifications of the proposed bands are enumerated in Table 1. According to these specifications, the parameters for the low-pass prototype were established; additionally, the group delays (τ) for these bands were computed, as presented in Table 2.

TABLE 1. Characteristics of the proposed dual-band bandpass filter.

Parameter	Value	Parameter	Value
f_{01}	2.390 GHz	RL_1	−23 dB
f_{02}	5.105 GHz	RL_2	−24 dB
Δ_1	3.77%	N_1	1
Δ_2	2.55%	N_2	1

TABLE 2. Calculated parameters of the proposed DB BPF.

Parameter	Value	Parameter	Value
g_o	1	M_{s1}	0.12166
g_1	2.25210	M_{1L}	0.12166
g_2	1	τ	0.703

f_{01} and f_{02} represent the center frequencies, while Δ_1 and Δ_2 express the fractional bandwidths of band1 and band2, respectively. RL_1 and RL_2 denote the return loss levels of band1 and band2; and N_1 and N_2 define the orders of the first and second bands, respectively. The coupling matrix ([**M**]) components depend on the FBW.

Subsequently, M_{ij} is obtained by applying Eq. (1).

$$M_{ij} = \frac{f_o}{BW}\frac{f_m^2 - f_e^2}{f_m^2 + f_e^2} \tag{1}$$

where BW is the operational bandwidth, f_0 the CF, and f_e and f_m are the electrical and magnetic resonance frequencies of the two connected resonators that can be determined via eigenmode analysis. According to [12], the rigorous group delay approach is typically employed in filter design to determine the necessary coupling between the input feed line and the first resonator (as well as the output feed line and the last resonator) in order to obtain the necessary FBW with the optimum impedance matching. The following equation is used to compute the value τ mathematically:

$$\tau\left(w_o\right) = \frac{4}{\omega_2 - \omega_1}\frac{1}{R} \tag{2}$$

where R is the normalized input impedance and output impedance, and ω_1 and ω_2 refer to the limits of BW. g_i is the ith low-pass prototype paramete; τ is the group delays; M_{ij} is the coupling element between resonators i and j. Moreover, S refers to the source while L refers to the load. The upcoming subsections will introduce the practical implementation of the previously described parameters.

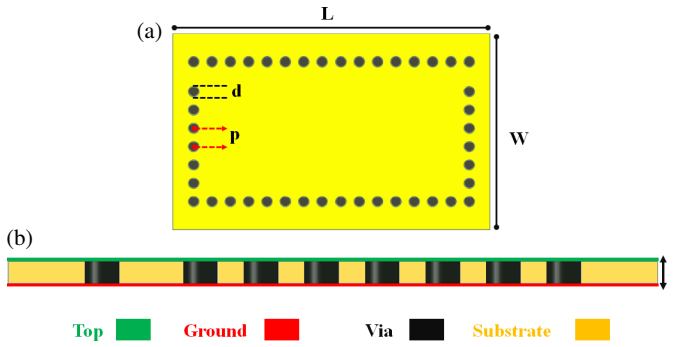

FIGURE 1. Suggested SIW resonator, (a) view top layer, (b) side view.

2.1. The SIW Resonator Proposed

The suggested SIW resonator was constructed on a Rogers RO4350 substrate, characterized by a dielectric constant (ε_r) of 3.66, a thickness (h) of 0.508 mm, and a loss tangent ($\tan\delta$) of 0.004. The resonator has a physical length (L) and width (W), forming a square-shaped cavity as shown in Figure 1. The cavity sidewalls were realized using metallic vias of diameter $d = 0.4$ mm, arranged with a pitch distance $p = 1.4$ mm and calculated from Eq. (3). The effective width (W_{eff}) and effective length (L_{eff}) of the SIW cavity were obtained using Eqs. (5) and (6), respectively [13]

$$p \leq 2d \tag{3}$$

$$f_c = \frac{c}{2W\sqrt{\mu_r \varepsilon_r}} \tag{4}$$

$$W_{eff} = W - \frac{d^2}{0.95 \times p} \tag{5}$$

$$L_{eff} = L - \frac{d^2}{0.95 \times p} \tag{6}$$

The Eigenmode simulation, an integrated tool inside Ansys EDT, was employed to analyze the first two natural modes of the SIW cavities, which would inform the design of the suggested passbands. For dimensions $L = 22.2$ mm and $W = 13.3$ mm, the SIW resonator exhibits TE_{10} and TE_{20} modes at frequencies of 8.6 GHz and 10.8 GHz, respectively, with an unloaded quality factor (Qu) of 250 for each band. The distribution of the electric field (E-field) for these modes is seen in Figures 2(a) and 2(b), respectively.

The modes can be excited from the same side, and yet distinct perturbation mechanisms can be utilized to independently modify their frequencies. The TE_{10} mode can be significantly perturbed when the SIW resonator is loaded at the center, while the TE_{20} mode can be adjusted if the perturbation is applied near the corners of the SIW cavity. This resonator will be utilized in the subsequent subsections to construct the final resonator.

The appropriate selection of the slot's form and dimensions can markedly decrease the resonance frequency and enable independent modulation of various modes.

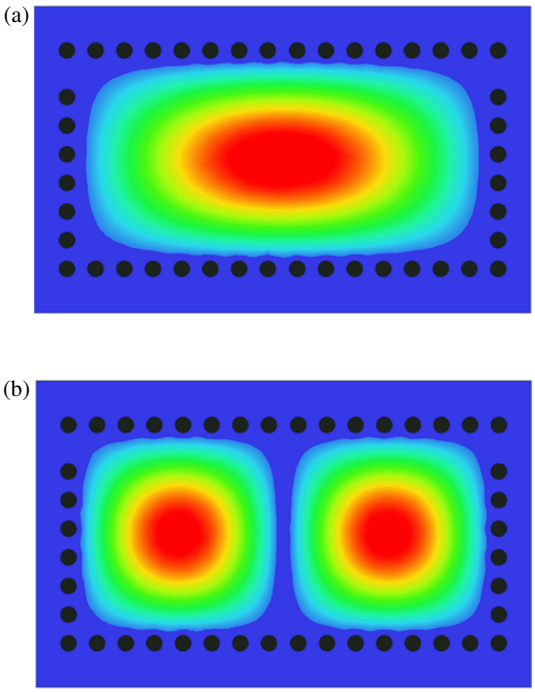

FIGURE 2. Electric field distribution of (a) TE_{10} and (b) TE_{20} mode.

2.2. Proposed SIW Resonator Loaded Complementary Split Ring Resonators (CSRRs)

The upper layer of the SIW can be efficiently loaded by a slot-like resonator. This slot functions as a control means whereby such effects can be utilized in specific shapes and locations. One of the most suitable choices is to use Complementary Split Ring Resonators (CSRRs). In this paper, a modified CSRR is incorporated to generate two bands, then reducing the overall filter size by applied SIW technique and to considerably shift down the resonance frequencies of TE_{10} mode and TE_{20} mode.

The modified CSRR forms a pair of coupled electric LC modes, which load the SIW cavity, with an electrically large size due to the meandering effect; hence, multi-reconfigurable bands were achieved within the proposed structure. The SIW cavity was loaded with two symmetrical CSRRs as mentioned in [14]. Two identical CSRRs were used for many reasons, since a SIW cavity has multiple modes where each mode has a different field distribution, and the usage of two different meander slots allows more degree of freedom to strongly perturb the largest number of these modes independently. Figure 3(a) determines the incorporation of the CSRR within the SIW resonator, and Figure 3(b) shows the design parameters of the proposed CSRR. To evaluate the effect of the CSRR, multiple eigenmode analyses were conducted by altering the geometric parameters of the proposed CSRR.

The impact of the parameter of the distance between the ends of the slot (W_3) on the first resonance mode 1 (fr_1) and the second resonance mode 2 (fr_2) is illustrated in Figure 4. The variation of W_3 from 0.5 mm to 7 mm increased fr_1 and fr_2 toward the higher frequencies. However, W_4 showed a different performance, which is shown in W_3, since increasing W_4 led to in a large increase in fr_2, while fr_1 was marginally es-

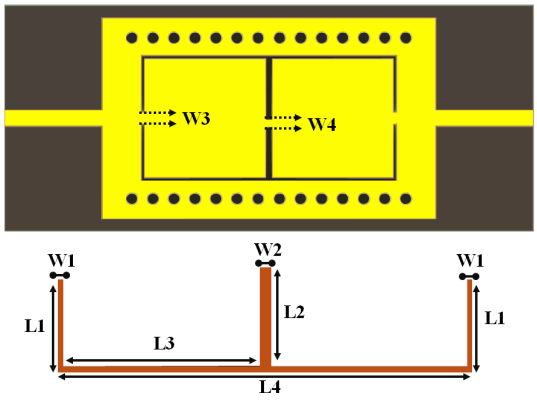

FIGURE 3. The proposed SIW loaded with CSRR, (a) top view and (b) CSRR parameters of the proposed resonator.

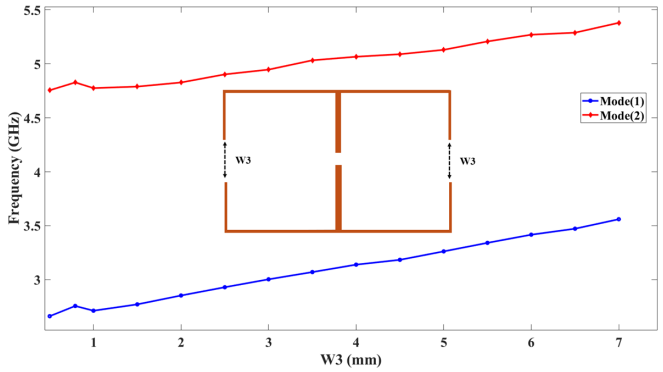

FIGURE 4. Resonance frequencies variation vs. W_3.

calated. The distance of the gap in the slot at the center of the resonator (W_4) was varied from 0.5 mm to 7 mm, causing fr_2 shifted toward higher frequency, but fr_1 stays without change as depicted in Figure 5.

The optimal dimensions of the proposed CSRR were the length of the slot at the edge of the resonator (L_1) = 3.75 mm, the width of the slot at the edge of the resonator (W_1) = 0.2 mm, the length of the slot at the center of the CSRR (L_2) = 4.03 mm, the width of the slot at the center of the CSRR (W_2) = 0.43 mm, the distance between the slot at the center of the resonator and the slot at the edge of CSRR (L_3) = 8.09 mm, and the total horizontal length of the CSRR (L_4) = 17 mm, as depicted in Figure 3. The CSRR slot is located at a distance of 8.5 mm from the edge of the SIW. Eigenmode simulation was performed on the finalized SIW-CSRR to equal to the resonance frequencies with quality factors. The initial mode resonates at 2.67 GHz has Qu 268, and the upper mode resonates at 4.7 GHz with Qu equal to 271, respectively, as depicted in Figure 6.

2.3. Reconfigurable Dual-Band SIW Filter

SIW is used in our design depicted in Figure 7, where the overall design contains two coplanar-waveguide feed ports and a CSRR slot, a middle layer made of a Rogers RO4350 substrate ($\varepsilon_r = 3.66$, $\tan\delta = 0.004$) that is 0.508 mm thick and includes multiple 0.4 mm-diameter vias spaced 1.4 mm centre-to-centre, and a bottom metallic layer that serves as the ground. The de-

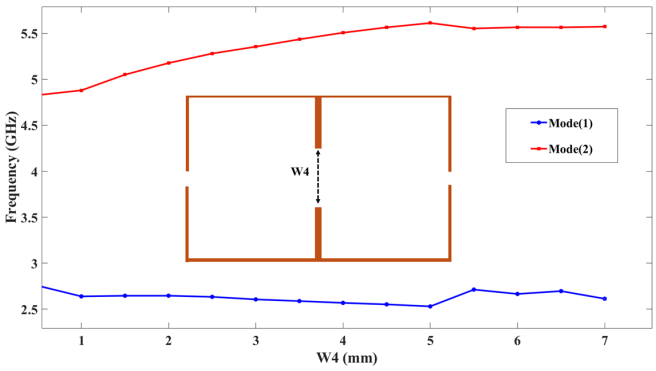

FIGURE 5. Resonance frequencies variation vs. W_4.

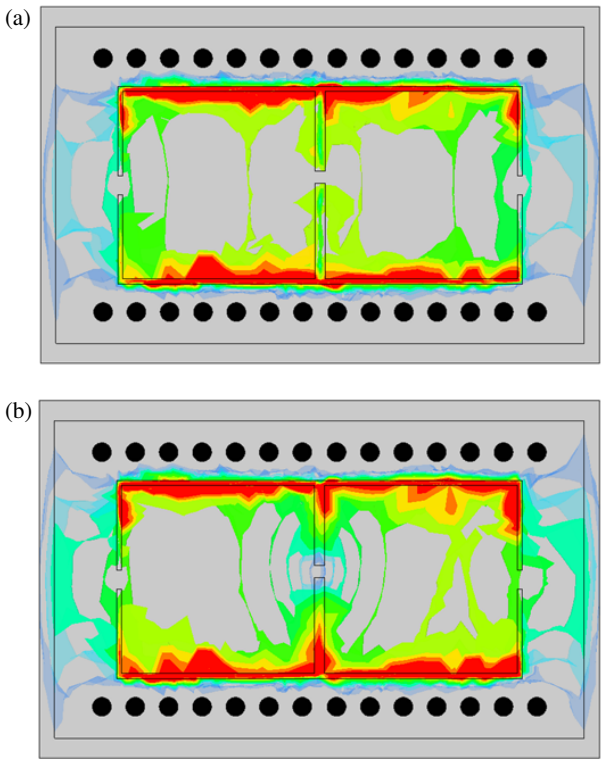

FIGURE 6. Shown EM-field distribution, (a) 1st resonance mode and (b) 2nd resonance mode.

sign was simulated using the High-Frequency Structure Simulator (HFSS), a commercial finite-element electromagnetic solver. A prototype was fabricated and tested, and the measured results showed good agreement with the simulated response, which is slightly different in some cases. The filter exhibits two passbands centred at 2.7 GHz and 4.7 GHz with the insertion losses approximately 1.5 dB and 1 dB for the lower and upper bands, respectively.

Moreover, the RL exceeds 14 dB across both bands. The isolation between the passbands is more than 10 dB, and the out-of-band rejection is greater than 20 dB. It is worth noting that, to the best of our knowledge, it is the first time that a diode has been placed within the same slot and controlled the current redistribution process to achieve the reconversion of a filter tunning, which simplifies the process of controlling the current

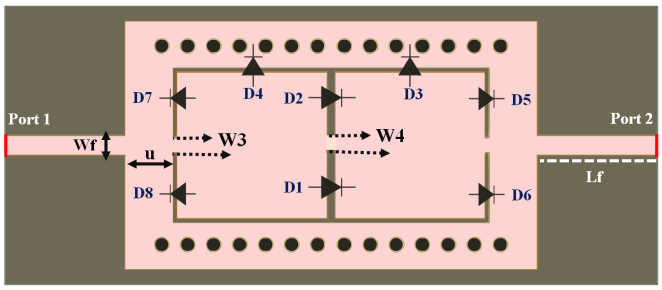

FIGURE 7. Input and output feeding mechanism of the top view of the structure.

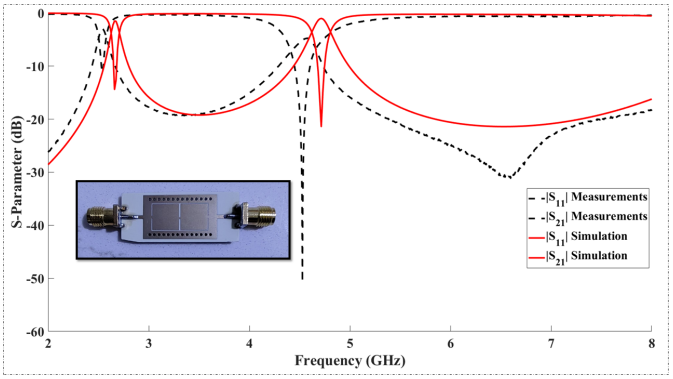

FIGURE 8. A standard proposed design where all diodes were OFF.

distribution and facilitates the manufacturing process due to the lack of other additions to the basic design, with the new reconfigurable mechanism introduced in the SIW structure. Unlike previous works, the PIN diodes in this filter are embedded directly inside the slot, rather than mounted on the resonator edges. This unique placement plays a fundamental role in enabling multiple degrees of reconfigurability. However, the filter provided independent tunability at the two passbands, allowing each band to shift in frequency without disturbing the other, an ability that is not commonly achieved in dual-band SIW filters. The proposed structure also offers bandwidth reconfigurability, where the effective coupling changes according to the diode switching cases, enabling controlled expansion or contraction of the bandwidth. Additionally, the configuration of the diodes inside the slot introduced a tunable cross-coupling effect, which resulted in controllable transmission zeros. Overall, the contribution of this work lies in the introduction of a compact, fully reconfigurable SIW bandpass filter capable of simultaneous tuning in: Center frequency, Fractional bandwidth, Transmission-zero locations.

It was supposed to use a diode with a forward bias resistance of less than 0.5 ohm, a reverse bias capacitance of 0.02 pf, and a total diode size not exceeding 0.2 mm. Due to the unavailability of these characteristics in the electronic circuit manufacturing market, the diode was replaced with a metal piece. When the forward bias is applied, the piece is placed, and when the reverse bias is applied, it is removed. Therefore, four models of the same filter were manufactured, each model representing one of the four cases, which will be listed in detail later. To realize a reconfigurable dual-band bandpass filter as depicted in Figure 7, eight PIN diodes are organized; the diodes are numbered from 1 to 8; and each diode has a specific, precisely calculated location to provide the best filter response.

These diodes are manipulated each time to achieve a reconfigurable BPF, and the f_o, Insertion Loss (IL), RL, FBW, and BW are also calculated for both the simulation and manufacturing stages, and the two stages are compared. This paper will only calculate four out of eight possible cases in this design.

Case 1: The first case serves as a Benchmark Point for the remaining cases, where the shifting at the operating frequency (f_o) is compared to other subsequent possibilities. In these cases, all diodes are in the OFF state, where f_o of the lower band (B1) was centered at 2.7 GHz and the f_o of higher band (B2) centered at 4.7 GHz, with IL less than 1.5 dB and 1 dB of B1 and B2, respectively, RL more than 14 dB for both B1 and B2, FBW 3.37% (BW: 90 MHz) of B1, and FBW equal to 4.45% (BW: 210 MHz) of B2.

The measurement results for this case are shown in Figure 8, where f_o of B1 was centered at 3.5 GHz with FBW equal to 5.86% (BW: 205), B1 had $IL < 2.5$ dB and $RL > 11.3$ dB, while the f_o of B2 is centered at 5.42 GHz with FBW equal to 7.47% (BW: 405 MHz), where B2 had less than 2.4 dB and more than 45 dB of IL and RL, respectively. This difference in the shift is mainly attributed to practical fabrication issues rather than to the ideal field distribution alone. In the fabricated prototype, the amount of solder used around the connector and RF connector, together with the actual conductor losses in the copper traces and connector, slightly modifies the effective cavity parameters, leading to the observed frequency shift. Nevertheless, the field distribution observed in Figure 9(a) shows that the current is concentrated in the red region, while the other regions are less confined around the CSRR slot.

Case 2: In this case, D_1 was ON and remaining diodes (D_2–$D_{7)}$ still OFF; B1 was moved slightly backward from 2.70 GHz to 2.57 GHz, while B2 moved toward higher frequency from 4.7 GHz to 5.24 GHz; the FBW was 3.49% (BW: 90 MHz) and 5.53% (BW: 290 MHz) of B1 and B2, respectively, with RL > 13 dB, IL < 1.58 dB, RL > 18 dB, and IL < 1.16 of B1 and B2, respectively. The measurement results showed that f_o was at 2.56 GHz of B1 and 5.23 GHz of B2. The FBW equals 1.71% (BW: 44 MHz) of B1, while the FBW is 5.33% (297 MHz) of B2, as shown in Figure 10. The field distribution in Figure 9(b) shows that the red regions appear in CSRR's center, where the green line becomes more vertical on CSRR slot, which ensures the rearranged currents inside the proposed filter when D_1 is activated.

Case 3: when $D_{1\&2}$ are activated, while D_{3-8} remain inactive, the f_o of B2 moves towards 5.47 GHz, while B1 remains at its standard (default) state of 2.7 GHz, which is equivalent to a frequency range of 0.77 GHz, giving the impression that this state represents an independent tuning for B2. As for FBW, it was 3.48% equivalent to 90 MHz for B1 and 4.84% equivalent to 320 MHz for B2. Meanwhile, the RL was > 14.16 dB with an IL > 1.5 dB, and the RL was greater than 18.14 dB with an IL less than 1.4 dB for both B1 and B2. Figure 11 shows the measurement results of the prototype, where the FBW was 5%, equivalent to 127 MHz, with an RL more than 11 dB and

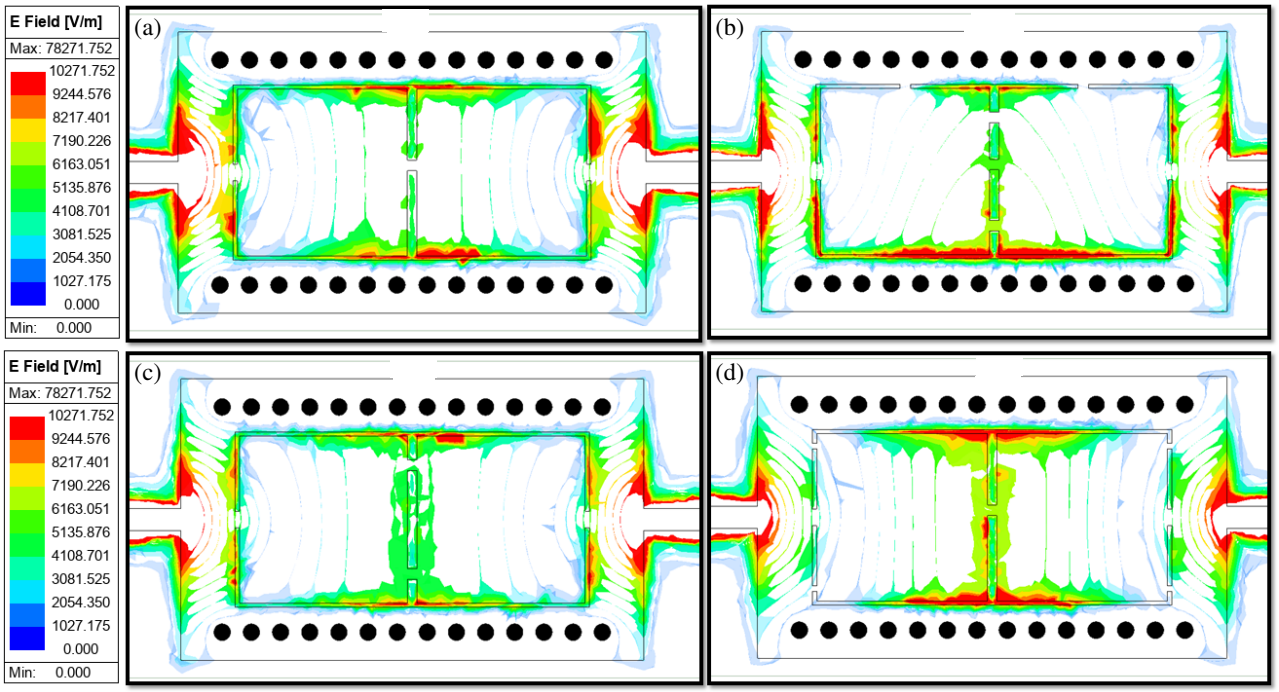

FIGURE 9. The distribution of electromagnetic currents in the four cases: (a) Case 1, when no diode is active, (b) Case 2, when only D_1 is active, (c) Case 3, when just two diodes are ON, (d) Case 4, when four diodes are ON.

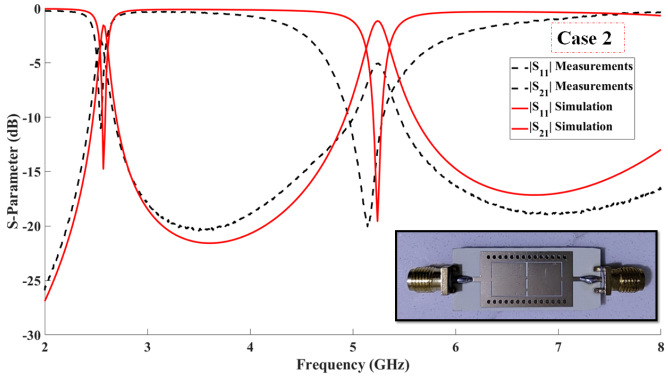

FIGURE 10. The S-parameter when D_1 and remined diodes was OFF.

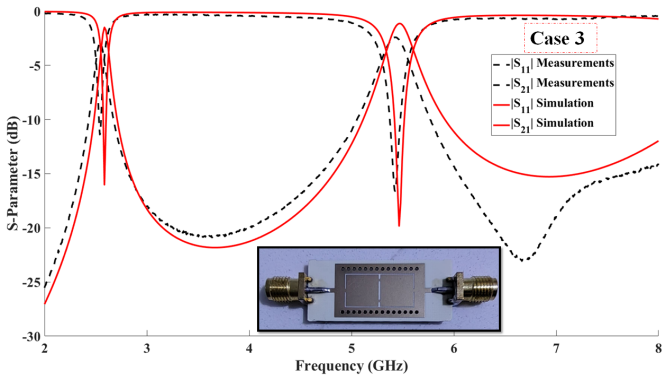

FIGURE 11. S-parameter when $D_{1\&2}$ were ON and remaining diodes (D_3–D_8) still OFF.

an IL less than 2.9 dB at an f_o of 2.54 GHz of B1. Nevertheless, for B2, at an operating frequency of 5.42 GHz, the FBW was 6.02%, equivalent to 326 MHz, with an RL $>$ 16 dB and an IL $<$ 2.39 dB. Figure 9(c) shows the electric-field distribution, where the field is strongly concentrated along the edges of the CSRR cavity and around the central slot resonator, indicating that these edges form the main resonant path that carries most of the energy. Inside the CSRR slot, the field lines extend smoothly from the left port to the right port with an almost symmetric distribution about the filter's center axis.

Case 4: In the final case, D_{1-4} are ON while D_{5-8} are OFF. In this state, B1 is shifted from 2.7 to 3.92 GHz, i.e., by about 1.25 GHz shifting frequency in this band, and B2 moves from 4.7 to 6.37 GHz, corresponding to a shift of about 1.65 GHz. The FBW is 3.32% (BW $=$ 130 MHz) and 9.09% ($BW = 580$ MHz) for B1 and B2, respectively. Moreover, B1 exhibits RL $>$ 12 dB with IL $<$ 2.31 dB, while B2 shows RL $>$ 18 dB with IL $<$ 1.1 dB, as presented in Figure 12. In the measured results, B1 has an FBW of 4.37% (BW $=$ 171 MHz) with RL $>$ 10 dB and IL $<$ 3.4 dB at $f_o = 3.91$ GHz; similarly, B2 has an FBW of 6.01% (BW $=$ 383 MHz) with RL $>$ 24 dB and IL $<$ 2.4 dB at $f_o = 6.37$ GHz. The electromagnetic field for this case is shown in Figure 9(d), where the current density is concentrated around the CSRR slots in the red regions.

Figures 13 and 14 show the measurement and simulation results for the S-parameter, demonstrating the degree of agreement, with slight differences due to manufacturing losses and losses resulting from the use of solder and glue in the model-making process. The filter was manufactured according to each case studied. Overall, the highest value for S_{11} was above

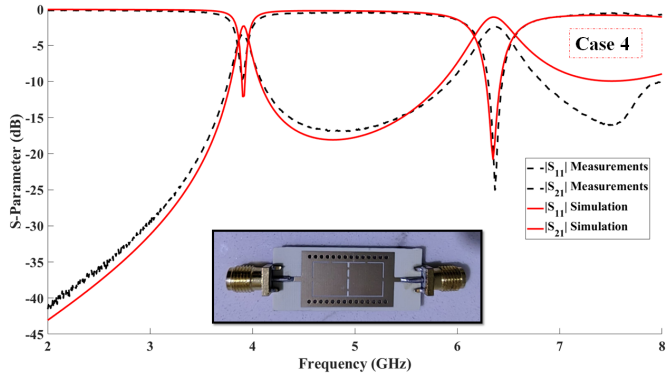

FIGURE 12. S-parameter when D_{1-4} were ON and remaining diodes (D_5–D_8) still OFF.

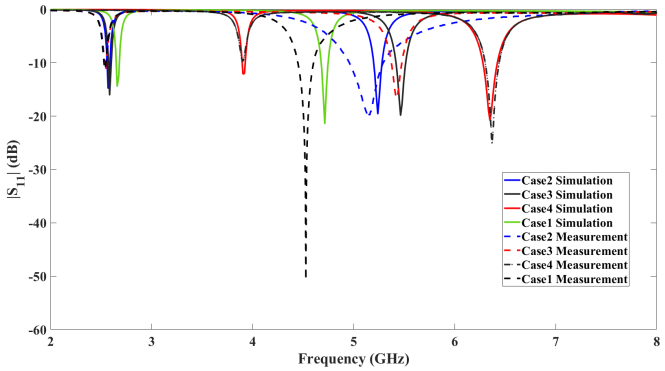

FIGURE 13. Return loss for all states (simulations and measurement results).

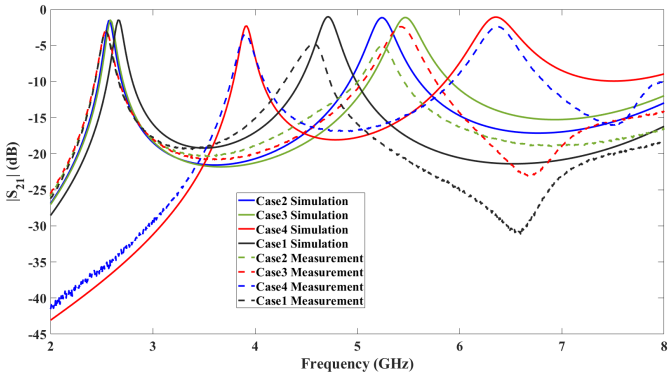

FIGURE 14. Insertion losses for all states (simulation and measurement results).

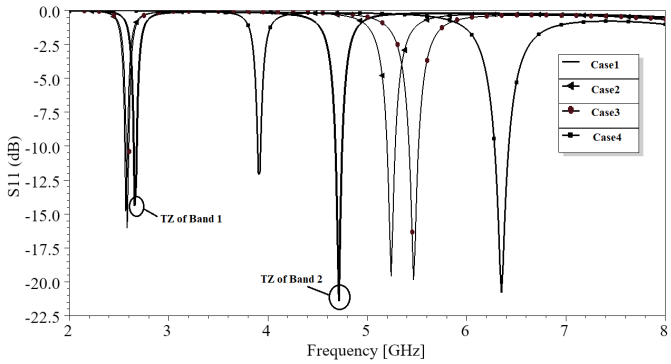

FIGURE 15. Reconfigurable transmission zero characteristics under different diode switching states.

45 dB. As for the insertion losses, B1 had a value of 3.4 dB in the worst case and 5 dB for B2. The frequency band ranged from 1.74% (90 MHz) to 6.03% (211 MHz) for the first band, while in the second band at high frequencies it ranged from 4.45% (210 MHz) to 9.09% (580 MHz). Finally, it is important to note that the frequency range covered by the model ranges from 2.5 GHz to 3.91 GHz for the first band and from 4.72 GHz to 6.37 GHz for the second band, which means that the filter has achieved the characteristic of a multi-application model.

2.3.1. Bandwidth Reconfigurability of the Proposed Filter

Variations in the bandwidth through different switching cases were mainly caused by the change of the electromagnetic coupling among SIW slots. PIN diodes were embedded directly inside the cavity, and their switching case modifies how strongly that the cavities interact with each other. If a diode was turned ON, it was provided an additional conductive path across the cavity, which increases the effective coupling among the resonators. Stronger coupling naturally results in a wider passband, but on the other hand, when the diode was turned OFF, this conductive contribution was removed; the coupling became weaker; and then the passband became narrower. Moreover, this trend is clearly reflected in the fractional bandwidth of the 2nd passband, where the bandwidth increases when the number of activated diodes increases. This further supports the conclusion that the diode switching cases provide a controllable mechanism for adjusting the bandwidth. In Case 1, the FBW of the 2nd passband was 4.45%. When the number of active diodes increased to two in Case 2, the FBW increased to 5.53%. The same is in Case 3, that with three active diodes, the FBW further increased to 5.85%. Finally, in Case 4, the FBW reached 6.37% when the number of active diodes increased to four.

2.3.2. Analysis and Control of Transmission Zeros of Proposed Filter

The transmission zeros (TZs) in the proposed dual-band SIW filter are mainly generated by the slot-based cross-coupling between the input and output ports. Since the PIN diodes are embedded inside the slot, their ON/OFF states directly modify the effective coupling path responsible for the signal cancellation and thus influence the locations of the TZs. As the diode configuration changes from Case 1 to Case 4, the lower and upper TZs shift in frequency accordingly.

For example, in Case 1, the lower TZ is located around 2.66 GHz, and the upper TZ appears near 4.715 GHz, while in Case 2, these TZs move to approximately 2.57 GHz and 5.24 GHz, respectively. Similar shifts were observed in Cases 3, since TZ at B1 was 2.585 GHz and 5.465 GHz at B2. In Case 4, TZs were located at 3.905 GHz and 6.35 GHz for B1 and B2, respectively. As more diodes are activated, the positions of the TZs can be tuned in a controllable way by adjusting the diode switching states. This controllable movement of the transmission zeros enhances the selectivity at both sides of the pass-

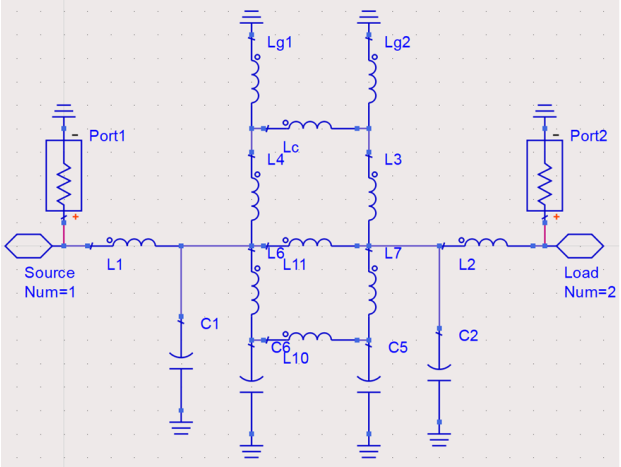

FIGURE 16. Equivalent circuit of the proposed filter.

bands, and the corresponding behavior can be clearly observed in Figure 15.

2.4. Equivalent Circuit of Proposed Design

The proposed lumped-element equivalent circuit model for the band-pass filter is shown in Figure 16. The metallic via on the SIW wall is modeled as the inductance L_g. The input microstrip line coupled to the resonators is represented by $L_{1\&2}$ and $C_{1\&2}$. Each CSRR-slot arm (the conducting paths surrounding the aperture) behaves as a resonator inductance $L_{6\&7}$, while $C_{5\&6}$ denotes the capacitance coupled to ground through the side openings W_3. The path between the strip and via wall is modeled as $L_{3\&4}$, and the narrow section above the via wall/central stem of the CSRR is modeled as L_c. The coupling between the two facing resonators occurs through the capacitance L_{10} (across the central gap) and magnetic coupling L_{11}. The response of the equivalent circuit is shown in Figure 17.

3. PROPOSED RECONFIGURABLE FILTER ANALYSIS

The optimised elements of the proposed filter were assembled to construct the final filter. To examine the independence of each passband, two different parametric experiments were conducted, and the results are depicted in Figures 4 and 5. The initial analysis, seen in Figure 4, was conducted by altering W_3. B1 and B2 exhibit corresponding alterations. The second analysis involved adjusting W_4 while maintaining a constant value for B1, with B2 changing subsequently and independently, as depicted in Figure 5. To guarantee a reflection-free transmission of electromagnetic waves at both ends of the filter, it was essential to adjust the width and length of the inset feed.

To accurately represent the electrical behavior of the proposed filter, its structural components must be defined for the development of an equivalent circuit model. Figure 7 shows the proposed SIW CSRR BPF structure with parameters under study noted as W, W_f, and L. The optimized parameters of the proposed filter are demonstrated in Table 3. The overall size of the 1st order DB SIW CSRR Slot BPFs was 21 mm $\times$ 34 mm. The realized bands were centered at 2.4 GHz and 5.1 GHz, and

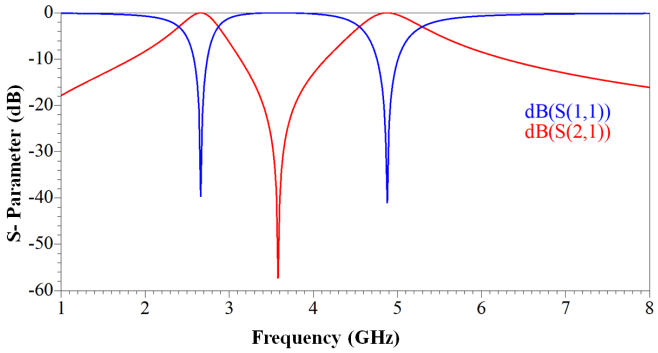

FIGURE 17. LC circuit S-parameter of dual-band BPF.

TABLE 3. Final dimensions of proposed dual-band CSRR slot filter in (mm).

Par.	Value	Para	Val	Para	Val	Par.	Val
W	13.34	W_f	1.07	L_3	3.75	d	0.4
W_1	0.2	W_4	0.5	L_4	8.084	P	1.4
W_2	0.43	L_1	3.75	L_f	6.5	L	22.2
W_3	0.79	$L2$	4.23	h	0.508	u	2.72

the RL was determined to be better than 20 dB overall in all four cases.

The IL of all four states at the first passband was found to be 1.5 dB ($<$ 2.5 dB in measurement results), while it was less than 1 dB ($<$ 2.4 dB on measurements) at the second passband, as shown in Figure 14. The 3-dB FBW was changed from 6.25% to 8.8% (5.98%–9.35% on measurements) at B1 and 6.63% to 7.72% at B2 (1.92%–4.48% in measurements) equivalent to a BW of 220 MHz to 250 MHz (210 MHz–266 MHz in measurements) at B1 and 320 MHz to 470 MHz (109 MHz–271 MHz in measurements) at B2. The E-feild distribution throughout the proposed design was plotted at different frequencies to further validate the operation principle. Figure 9 illustrates the E-field in all cases.

4. SIMULATION AND MEASUREMENT FOR THE PROPOSED SIW-MSL BPF

The fabricated model of the proposed SIW CSRR Slot BPF is shown in Figure 18, where this prototype was analyzed utilizing Keysight/Agilent Technologies E5071C vector network analyzer (VNA). The validations for the design could be shown through the measurement result in Figures 13 and 14. The figures exhibit that the filter's response had two passbands. The 1st band had a CF at 2.67 GHz, and FBW was changed from 1.71% to 5.86%, equivalent to a BW of 44 MHz–205 MHz.

The RL is better than 11 dB with an IL about 2.5 dB. Additionally, the second band operates at a CF of 5.42 GHz with the variation of FBW 5.33%–7.47% equivalent to a BW 297 MHz–405 MHz with the IL less than 2.4 dB and RL more than 45 dB. The difference in IL level at the two bands is attributed to the impedance matching level at these bands where the first band shows an S_{11} level around 12 dB while the second band shows a

TABLE 4. The comparison of the proposed CSRR slot DB BPF with other works.

Ref.	F_o (GHz)	Tuning %	FBW %	S_{11} (dB)	S_{21} (dB)
[3]	2.4/3.5	15.9/9.85	NA	> 25	< 3.5
[15]	3.65/5.8	5.83/11.19	4.72/6.10	> 10	$< 2.9/< 2.1$
[16]	3.1/10.6	51.2	17.69	25	< 1.2
[17]	1.3/1.7	0.8/0.6	12/0.8	> 15	< 1.8
[18]	7.86/9.95	9/12.3	9.03/12.35	$> 14/> 12$	< 1.5
[19]	16.2/19.1	1.71/3.09	1.71/3.09	18/19.2	1.8/1.9
[20]	0.209/0.223	4.63/2.74	3.5/3.4	35.3	0.53/1.35
This Work	2.7/4.7	43.3/19.65	3.4 : 1/1.40 : 1	> 10	$< 3.4/< 5$

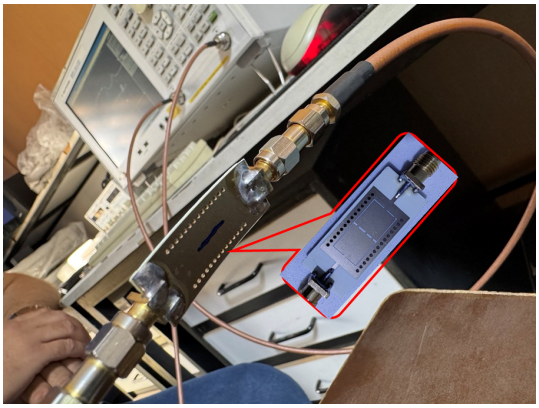

FIGURE 18. Measurements setup.

lower impedance matching level of $S_{11} = 20$ dB. Furthermore, as the second band operates at higher frequency band centered at 4.7 GHz, the electrical length of the filter is larger than its electrical length at the first band, which is centered at 2.7 GHz, so it is natural to experience higher IL level at the higher operating band.

Accordingly, the two factors contribute to the increase of the IL in the first and second bands. However, a better matching may enhance the IL. The minor discrepancy between the simulated and measured results was attributable to fabrication tolerances, material variability, and assembly misalignment. Table 4 shows the proposed CSRR Slot DB BPF with the most recent reconfigurable filters.

5. CONCLUSION

The proposed dual-band band-pass filter, functioning at 2.7 GHz for Bluetooth and 4.7 GHz for 5G and weather/navigation radars, exhibited efficient frequency management, compact size, and selectivity. This work has established those tuning mechanisms, including PIN, permits the independent control of two frequency bands, underlining flexibility for various mobile communication applications. The fabrication results agreed with simulations, demonstrating robust performance with minimal insertion loss differences and efficient out-of-band rejection. The developed filter presents a viable option for modern wireless communication systems, offering flexible performance and practical spectrum usage.

REFERENCES

[1] Al-Saedi, H., W. M. Abdel-Wahab, S. Gigoyan, and S. Safavi-Naeini, "SIW series-fed patch antenna array based on transverse slot excitation for millimeter wave (MMW) applications," in *2016 IEEE International Symposium on Antennas and Propagation (APSURSI)*, 1593–1594, Fajardo, PR, USA, 2016.

[2] Nwajana, A. O., A. Dainkeh, and K. S. K. Yeo, "Substrate integrated waveguide (SIW) bandpass filter with novel microstrip-CPW-SIW input coupling," *Journal of Microwaves, Optoelectronics and Electromagnetic Applications*, Vol. 16, No. 02, 393–402, 2017.

[3] Hussein, A. F., M. J. Farhan, and J. K. Ali, "Switchable/tunable dual-band BPF for bluetooth and 5G NR applications," *Progress In Electromagnetics Research C*, Vol. 152, 103–110, 2025.

[4] Zhu, L., R. R. Mansour, and M. Yu, "Triple-band cavity bandpass filters," *IEEE Transactions on Microwave Theory and Techniques*, Vol. 66, No. 9, 4057–4069, Sep. 2018.

[5] Mei, Y., B.-G. Liu, Y. Yi, H. Xu, and Y. Zhang, "Liquid metal frequency-reconfigurable siw bandpass filter based on gravity field," *Electronics Letters*, Vol. 57, No. 12, 481–482, Jun. 2021.

[6] Rahman, M. A. and P. Sarkar, "A tunable bandpass filter using modified half mode SIW cavity and spoof SPP structure," *International Journal of Microwave and Optical Technology*, Vol. 18, No. 2, 122–130, 2023.

[7] Mahdi, S. O., M. N. Raheema, and R. T. Hammed, "Design and analysis of reconfigurable filters employing varactor and PIN diodes," *Engineering and Technology Journal*, Vol. 43, No. 2, 115–136, 2024.

[8] Deng, M. and D. Psychogiou, "Tune-all substrate-integrated-waveguide (siw) bandpass filters," in *2019 14th European Microwave Integrated Circuits Conference (EuMIC)*, 322–325, Paris, France, 2019.

[9] Han, Y.-K., H.-W. Deng, J.-M. Zhu, S.-B. Xing, and W. Han, "Compact dual-band dual-mode SIW balanced BPF with intrinsic common-mode suppression," *IEEE Microwave and Wireless Components Letters*, Vol. 31, No. 2, 101–104, Feb. 2021.

[10] Xie, H.-W., K. Zhou, C.-X. Zhou, and W. Wu, "Compact SIW diplexers and dual-band bandpass filter with wide-stopband performances," *IEEE Transactions on Circuits and Systems II: Express Briefs*, Vol. 67, No. 12, 2933–2937, Dec. 2020.

[11] Zhu, Y. and Y. Dong, "A compact dual-band quasi-elliptic filter based on hybrid SIW and microstrip technologies," *IEEE Transactions on Circuits and Systems II: Express Briefs*, Vol. 69, No. 3, 719–723, Mar. 2022.

[12] Cameron, R. J., C. M. Kudsia, and R. R. Mansour, *Microwave Filters for Communication Systems: Fundamentals, Design, and Applications*, John Wiley & Sons, 2018.

[13] Al-Darraji, H. and H. Al-Saedi, "Compact dual-band BPF based on loaded SIW with meandered slot line for 5G and beyond applications," *Progress In Electromagnetics Research M*, Vol. 128, 89–98, 2024.

[14] Xiang, Q.-Y., Q.-Y. Feng, X.-G. Huang, and D.-H. Jia, "Substrate integrated waveguide filters and mechanical/electrical reconfigurable half-mode substrate integrated waveguide filters," *Journal of Electromagnetic Waves and Applications*, Vol. 26, No. 13, 1756–1766, 2012.

[15] Iqbal, A., J. J. Tiang, C. K. Lee, N. K. Mallat, and S. W. Wong, "Dual-band half mode substrate integrated waveguide filter with independently tunable bands," *IEEE Transactions on Circuits and Systems II: Express Briefs*, Vol. 67, No. 2, 285–289, Feb. 2020.

[16] Li, Q. and T. Yang, "Compact UWB half-mode SIW bandpass filter with fully reconfigurable single and dual notched bands," *IEEE Transactions on Microwave Theory and Techniques*, Vol. 69, No. 1, 65–74, Jan. 2021.

[17] Simpson, D. J., R. Gómez-García, and D. Psychogiou, "Single-/multi-band bandpass filters and duplexers with fully reconfigurable transfer-function characteristics," *IEEE Transactions on Microwave Theory and Techniques*, Vol. 67, No. 5, 1854–1869, May 2019.

[18] Fang, X., Y. C. Li, L. W. Li, W. Che, and Q. Xue, "A dual-band tunable balanced filter with independently tuning bands," *IEEE Transactions on Circuits and Systems II: Express Briefs*, Vol. 69, No. 4, 2076–2080, Apr. 2022.

[19] Kumar, C. S., R. Kumari, and H. V. Dixit, "Compact dual-band band-pass filter using single multimode SIW cavity with independent controllable fractional bandwidth," *International Journal of RF and Microwave Computer-Aided Engineering*, Vol. 2025, No. 1, 9968988, 2025.

[20] Zhu, B., D. Lu, M. Sun, and M. Yu, "Tunable dielectric filter and filtering power divider with multilevel transfer function tunability," *IEEE Transactions on Microwave Theory and Techniques*, Vol. 73, No. 8, 5133–5151, Aug. 2025.